JOURNAL OF CATALYSIS 151, 338–348 (1995)

Characterization and Oxidation Catalysis of Alkylaromatics over CVD Fe/Mo/Borosilicate Molecular Sieve: Fe/Mo/DBH

G. W. Zajac,* C. Choi-Feng,* J. Faber,* J. S. Yoo,†,[1] R. Patel,‡ and H. Hochst‡

*Amoco Corporation, P.O. Box 3011, Naperville, Illinois 60566-7011; †Amoco Oil Company, H-2, P.O. Box 3011, Naperville, Illinois 60566-7011; and ‡Synchrotron Radiation Center, Stoughton, Wisconsin 53589

Received May 3, 1994; revised September 12, 1994

The Fe/Mo/DBH catalyst exhibited stable *p*-selective oxidation activity in forming terepohthaldehyde by gas-phase O_2 oxidation of *p*-xylene under mild reaction conditions with high selectivity. It also catalyzes other reactions such as oxydehydrogenation, hydroxylation of benzene to phenol, and CO_2 activation. The catalyst was characterized by employing combined techniques of Raman spectroscopy, analytical electron microscopy (AEM), high-resolution electron microscopy (HREM), Raman spectroscopy, X-ray powder diffraction, X-ray photoelectron spectroscopy, and *in situ* total electron yield near edge spectroscopy (XANES). Two phases, $Fe_2(MoO_4)_3$ and MoO_3, were identified by Raman spectroscopy. *In situ* low-temperature CO_2-dosing XANES experiments provided evidence for a strongly chemisorbed CO_2 species on Fe/Mo/DBH at the reaction temperature. © 1995 Academic Press, Inc.

INTRODUCTION

Terephthaldehyde emerges as an interesting bifunctional reactive intermediate for a variety of commercial applications including liquid crystals, electron conductive polymers, thermal engineering polymers such as polyimines, polystrylazines, and polybenzimidazoles, optical brightener, and other novel specialty polymers. It also serves as a starting material for the synthesis of specialty monomers such as cyclohexanedimethanol, *p*-hydroxybenzoic acid and hydroquinone, *p*-hydroxymethylbenzoic acid, and benzene dimethanol.

Conventionally, terepthaldehyde has been synthesized via hydrolysis of the di- and tetrachlorinated side-chain derivatives of *p*-xylene in the liquid phases (1). Thus, the price of terephthaldehyde, approximately $11–13/lb, becomes inhibitive for commercial use, although numerous applications have been identified. However, this situation may be changed by the advent of the Fe/Mo/borosilicate catalyst prepared by the chemical vapor deposition technique, CVD Fe/Mo/DBH. DBH is defined as a partially deboronated borosilicate molecular sieve, HAMS-1B-3.

p-Xylene was selectively oxidized to terephthaldehyde and *p*-tolualdehyde via gas-phase O_2 oxidation of *p*-xylene over CVD Fe/Mo/DBH under mild conditions (2). In a typical run at 355°C, selectivities of terephthaldehyde, *p*-tolulaldehyde, and CO_x were 56, 19, and 8.5 mol%, respectively, at the *p*-xylene conversion of 60%:

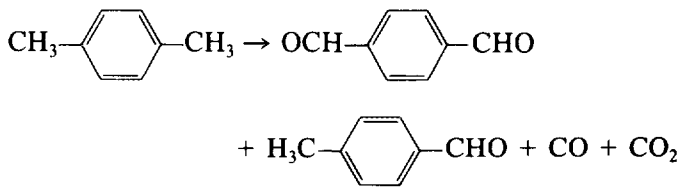

The yields of terephthaldehyde and *p*-tolualdehyde were remarkably improved at lower oxidation temperature in the presence of CO_2. In other words, CO_2 was activated on CVD Fe/Mo/DBH, and functioned as a cooxidant for the aldehyde synthesis (3).

p-Xylene was preferentially oxidized from the xylene isomer mixture containing ethylbenzene by utilizing the wide reactivity gap existing between *p*-xylene, on one hand, and *o*- and *m*-xylene and ethylbenzene, on the other, which originates from the *p*-selective property of the CVD Fe/Mo/DBH catalyst (4). Besides the syntheses of aldehydes, a variety of oxidation reactions were catalyzed with this catalyst (5).

It was learned that these interesting catalyses stemmed from the unique role played by the partially deboronated borosilicate molecular sieve matrix by examining various supporting matrices (6). We believe the supported ferric molybdate moieties formed upon prolonged calcination are a separate phase in intimate contact and anchored on the DBH matrix. Electron microscopy indicates that the deposition of Fe^{3+} and Mo^{6+} occurs within the channels of the DBH matrix initially. However, during the calcination process to form the active catalyst, migration of the ferric molybdate species occurs to the exterior of the channel structure of the DBH molecular sieve. The active catalytic sites for the oxidation of *p*-xylene are on the surface of the highly and uniformly dispersed ferric molybdate phase present exterior to the DBH framework.

[1] To whom correspondence should be addressed.

0021-9517/95 $6.00

TABLE 1

Compositions of CVD Catalysts 1–5, Fe/Mo/DBH, or ZSM-5

Catalyst ID	Metal composition (Mo wt%)	(Fe wt%)	(Mo/Fe)	Surface area (m^2/g)	Remarks
(1) CVD Fe/Mo/DBH	4.6	1.4	1.9	244	MoO_2Cl_2
(2) CVD Fe/Mo/DBH	5.2	1.5	2.1	288	$MoCl_5$
(3) CVD Fe/Mo/DBH	14.5	2.6	3.3	283	Dried precursor, MoO_2Cl_2
(4) CVD Fe/Mo/DBH	7.0	2.3	1.8		Prolonged calc'nd
(5) CVD Fe/Mo/ZSM-5	5.3	2.2	1.4		—
(6) CVD Fe/Mo–ZSM-5	8.9	2.5	2.0		Treated cat. 5 with ammonium paramolybdate

Molecular modeling with ferric molybdate species within the channels of the DBH indicates that insufficient space is available for the *p*-xylene molecule to react on interior of the DBH channels. These findings prompted us to investigate the structure of the CVD Fe/Mo/DBH catalyst by X-ray diffraction, X-ray photoelectron spectroscopy (XPS), electron microscopy, Raman spectroscopy (*in situ* and *ex situ*), and *in situ* synchroton radiation studies.

EXPERIMENTAL

Materials

Catalysts 1–6 were prepared according to the chemical vapor deposition procedure described elsewhere (2), and their compositions are summarized in Table 1.

Characterization of Catalyst

XPS and Raman Spectroscopy Studies

XPS. XPS spectra were recorded on a Perkin Elmer 5400 XPS spectrometer with a Mg$K\alpha$ X-ray ($h\nu$ = 1253.6 eV) at a takeoff angle of 45°. Quantitation is achieved by multiplexing all observable elemental core levels and applying a cross-section correction to the integrated intensities.

Raman spectroscopy. All Raman scattering measurement were carried out using the 514.5-nm line from an Ar ion laser, and a Jobin-Yvon Ramalor 1000 Raman spectrometer with a 2400 grooves/mm grating or a Dillor Omars 89 Raman spectrometer equipped with a multichannel detector. The laser beam intensity was typically 100–150 mW, and a sample spinner was used during analysis at a speed of ~3000 rpm. An Ar ion laser operated at a wavelength of 5145 Å and 25 mW was used for analysis. The sampling area was approximately 5–10 μm^2. All peak width and line positions were determined by a least-squares fit to a Lorentzian lineshape.

XRD, EM, and XANES Studies

X-ray diffraction. XRD was employed to study the starting ferric molybdate used to prepare a Fe/Mo/DBH catalyst. The motivation for this work centers on the experimental observation of significant catalytic activity, even at temperatures as low as 250°C. The XRD studies were partitioned into two distinct areas: a room-temperature study of the phases present in the starting material and a high-temperature study in the temperature range $20 < T < 450$°C. A small portion of the ferric molybdate sample was ground to a fine powder. Cu$K\alpha$ radiation was used. For the high-temperature work, the powder was slurried in alcohol and spread onto the heating strip of the Buhler high-temperature furnace attachment mounted on a Scintag PAD-X vertical goniometer diffractometer. The high-temperature sample was subjected to a 3×10^{-5} Torr vacuum for approximately 24 h at room temperature. The temperature-dependent work was done with Coleman instrument grade CO_2 flowing over the sample. The gas-flow rate was 100cc/min and was controlled by a mass flow controller.

Electron microscopy. To study the pathway for deposition and the distributions of Fe and Mo in the final CVD Fe/Mo DBH catalyst, two samples, fresh and calcined for a prolonged period, were characterized.

These samples were ground, embedded in LR-White resin, and cured for 60 min at 90°C. TEM thin sections were then obtained by ultramicrotomy, which were coated lightly with carbon prior to the EM examination. The thin sections were examined with a JEOL JEM 2000EX high-resolution electron microscope (HREM) and analyzed with a Philips 420 analytical electron microscope (AEM) which is equipped with a Noran 5502 energy dispersive X-ray emission spectrometry (EDXS).

XANES. The total electron yield experiments were performed in an ultrahigh vacuum system at the synchrotron radiation center (SRC), Stoughton, Wisconsin, managed by the University of Wisconsin, Madison, equipped

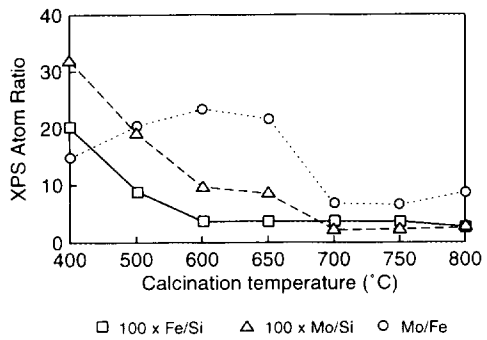

FIG. 1. Effect of calcination temperature on catalyst 1, 4.6 wt% Mo, 1.4 wt% Fe, Mo/Fe = 1.8, surface area 244 m^2/g.

with gas handling capability for controlled CO_2 dosing experiments of pure ferric molybdate (Alpha). CVD Fe/Mo deboronated molecular sieve catalysts were measured at the same time for comparison. The procedure required cooling the sample to 100 K followed by saturation coverage of 1×10^6 liters of CO_2. The sample was exposed to tuned synchrotron radiation at a series of temperatures from 100 to 603 K to simualte reaction temperatures (330°C).

The total electron yield core level spectroscopy was performed at the SRC on the 6-m toroidal grating monochromator. The three core levels of the carbon dioxide-dosed ferric molybdate which were measured were the carbon 1*s* (ca. 284 eV), the molybdenum $3d_{5/2,3/2}$ (ca. 232 eV), and the iron $2p_{3/2,1/2}$ (ca. 710 eV). The XANES measurements were performed at temperatures simulating catalytic reactions.

RESULTS AND DISCUSSION

XPS Study

The XPS study of catalyst 1, CVD Fe/Mo/DBH, containing 4.6 wt% Mo, 1.4 wt% Fe, and Mo/Fe = 1.90, with surface area of 244 m^2/g, was conducted and the surface composition was determined to be as follows:

Fe/Si		Mo/Si		Mo/Fe	
XPS	Bulk (ICP)	XPS	Bulk	Bulk	XPS
3.6	15.9	10.9	30.5	1.89	3.03

Catalyst 1 was calcined in air overnight at seven different temperatures from 400 to 800°C to determine the phase change occurring on the catalyst. The binding energies for Fe $2p_{3/2}$ (710.8 eV) and Mo$3d_{5/2}$ (232.1 eV) are virtually the same in the oxidized samples, and are consistent with Fe^{3+} and Mo^{6+}, respectively. No detectable binding energy shift was observed as a function of calcination temperature. Figure 1 shows the XPS atomic ratios of Fe/Si, Mo/Si, and Mo/Fe as a function of calcination temperature. The first two parameters are used as a measure of dispersions of Fe and Mo on the DBH support, whereas the last parameter is used to probe surface restructuring of Fe and Mo. In the temperature range of 400–600°C, both the Fe/Si and Mo/Si ratios are decreased, but in the temperature range 600–800°C, the Mo/Si ratio continues to decrease and eventually levels off above 700°C while the Fe/Si ratio remains essentially constant. This change also results in a lower Mo/Fe ratio, which is an important indicator for controlling the catalyst performance. The lowering in Mo/Si and Mo/Fe ratios observed by XPS can be attributed to sublimation of $MoO_3 \cdot H_2O$ during calcination at higher temperatures. This findings are substantiated by the MoO_3 crystals observed during the calcination pretreatment and the results of the Raman spectroscopic study discussed later.

XRD Study

The initial room-temperature results are illustrated in Fig. 2. A number of possible phases are indicated by the (Joint Committee on Powder Diffraction (JCPD)) patterns schematically illustrated in the bottom of Fig. 2. The vertical lines indicate the positions and integrated intensities of Bragg reflections obtained in the literature. Ferric molybdate and molybdenum trioxide phases are identified as illustrated in Fig. 2. Based on reference MoO_3 material, and the intensity of the observed MoO_3 Bragg peaks (e.g., at $2\theta = 23.7°$), approximately 15 wt% of the starting material belongs to this phase. In addition to this orthorhombic MoO_3 phase, two ferric molybdate phases were used to identify the Bragg peaks observed in Fig. 3. In both cases, the unit cell symmetry is monoclinic, but subtle differences in unit cell parameters differentiate these two phases as indicated in Table 2.

Figure 4 shows the results of a systematic *in situ* study

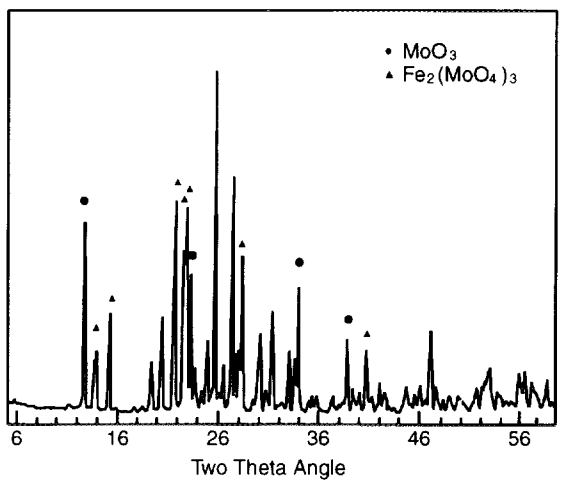

FIG. 2. XRD of $Fe_2(MoO_4)_3$ sample.

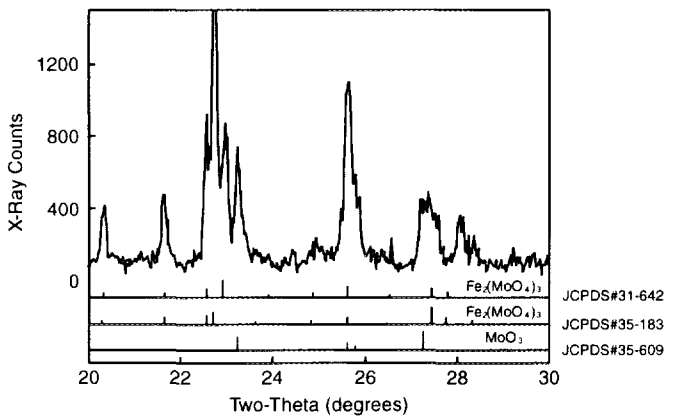

FIG. 3. Ferric molybdate X-ray powder pattern at T = 27°C.

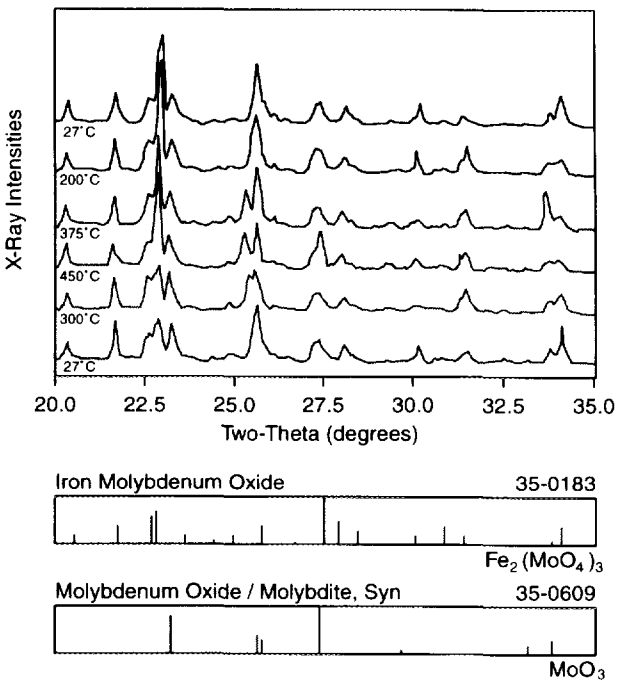

FIG. 4. *In situ* X-ray diffraction CO_2 calcinations indicating phase changes occurring by 300°C in ferric molybdate ($Fe_2(MoO_4)_3$).

of ferric molybdate in flowing CO_2 as a function of temperature. A phase transition is observed. The splitting of the Bragg peak at 2θ = 26° is perhaps the most obvious indicator of a change in symmetry of the ferric molybdate crystal lattice. The results were obtained on heating and cooling. The transition appears to be reversible. The transition begins at $T \sim$ 250°C and is not complete even at T = 450°C. A phase transition has been observed and reported in the literature. Massarotti *et al.* (7) have confirmed that a ferroelastic transition is observed in ferric molybdate, with T_c = 513°C (the heat of transition is 1966 J/mol). There is some indication in this work that the presence of MoO_3 might significantly alter T_c. Although the argument is unclear, Massarotti *et al.* point out that a deficiency of MoO_3 might occur in the high-temperature, paraelastic (orthorhombic structure) phase of ferric molybdate and that solubility of excess MoO_3 in ferric molybdate is not probable.

In the work reported here, we observe a transition toward the orthorhombic, ferroelastic phase of ferric molybdate. At the highest temperature investigated (T = 450°C), the transformation is not complete. The literature (8) suggests that the transition can be affected by various alterations to stoichiometry. Indeed, our observation that two ferric molybdate phases, with different stoichiometry, coexist at room temperature may be consistent with this idea. It is tempting to suggest that the unexpected activity of the Fe/Mo/DBH catalyst may be coupled with local stoichiometric disorder observed in this work.

Electron Microscopy Study

The typical microstructures of the two samples are shown in Fig. 5 (Fig. 5a, fresh CVD Fe/Mo/DBH as received, and Fig. 5b, CVD Fe/Mo DBH counterpart calcined for a prolonged period). At low magnifications, the molecular sieve particles in the fresh CVD Fe/Mo DBH appear to have a rather uniform contrast. Only at higher magnifications do very small dark particles begin to appear. The energy dispersive X-ray emission study (EDXS)

TABLE 2

JCPDS Diffraction Card File Index Numbers and Unit Cell Dimensions for the Detected Phases

Powder diffraction card file number		*a* (A)	*b* (A)	*c* (A)	β (degrees)
35-609	MoO_3	3.963	13.856	3.697	90
31-642	$Fe_2(MoO_4)_3$	15.65	9.2	18.2	125.6
35-183	$Fe_2(MoO_4)_3$	15.737(8)	9.231(5)	18.224(9)	125.4

Note. The numbers in parentheses are reported estimated standard deviations.

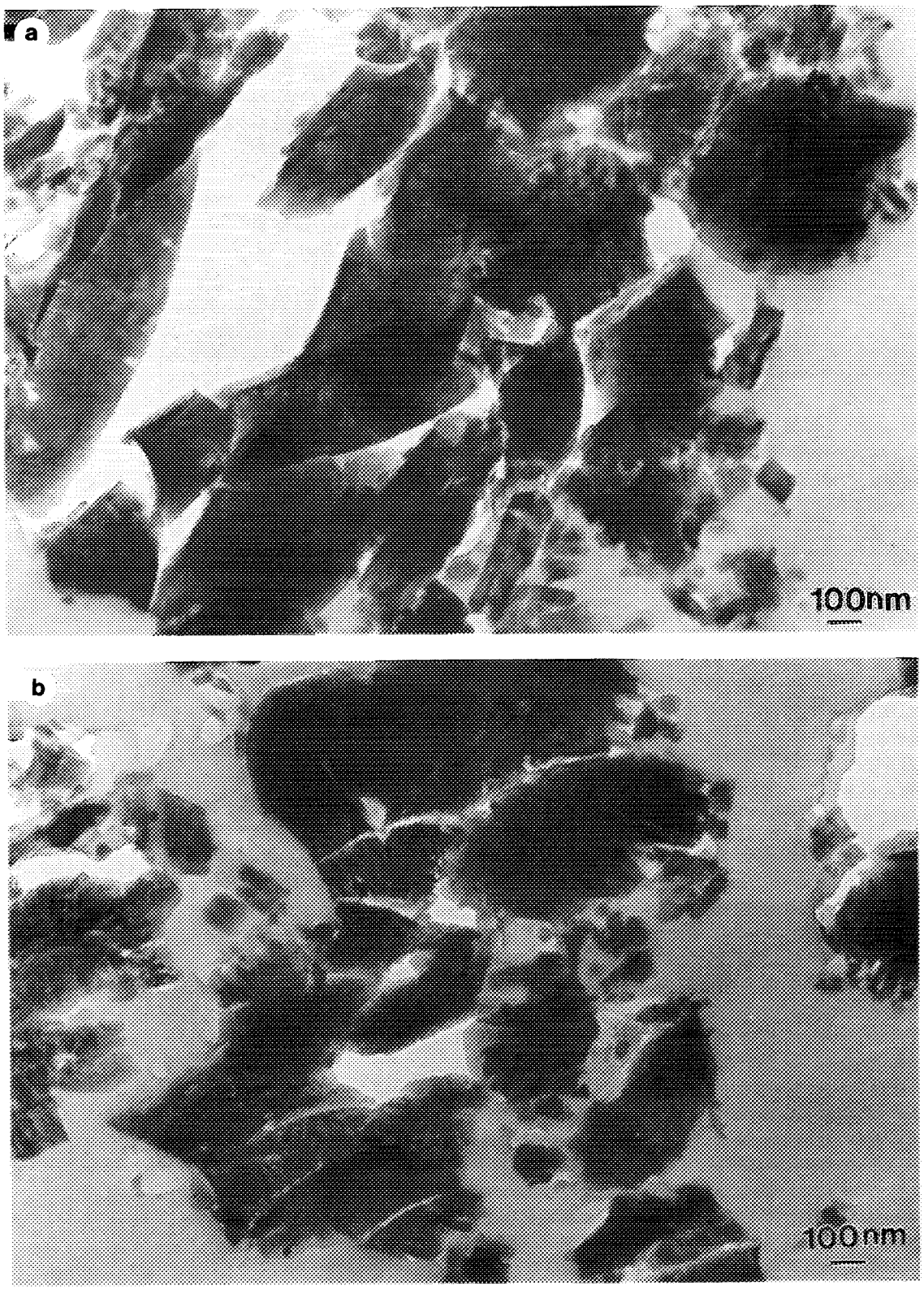

FIG. 5. Microstructure of CVD Fe/Mo/DBH; (a) fresh, (b) calcined at 650°C for a prolonged period.

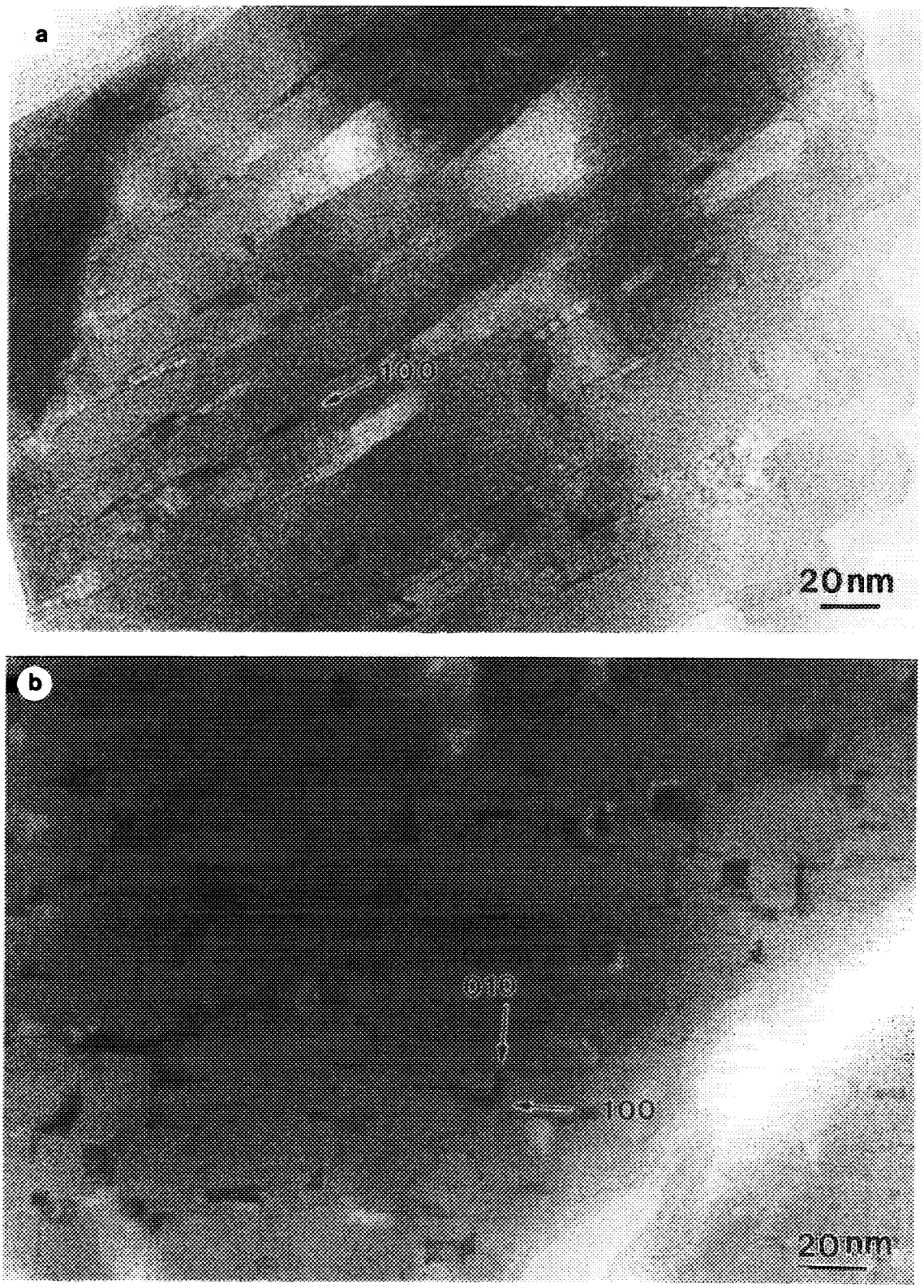

FIG. 6. High resolution electron micrographs of CVD Fe/Mo/DBH; (a) fresh, (b) calcined, at 650°C for a prolonged period.

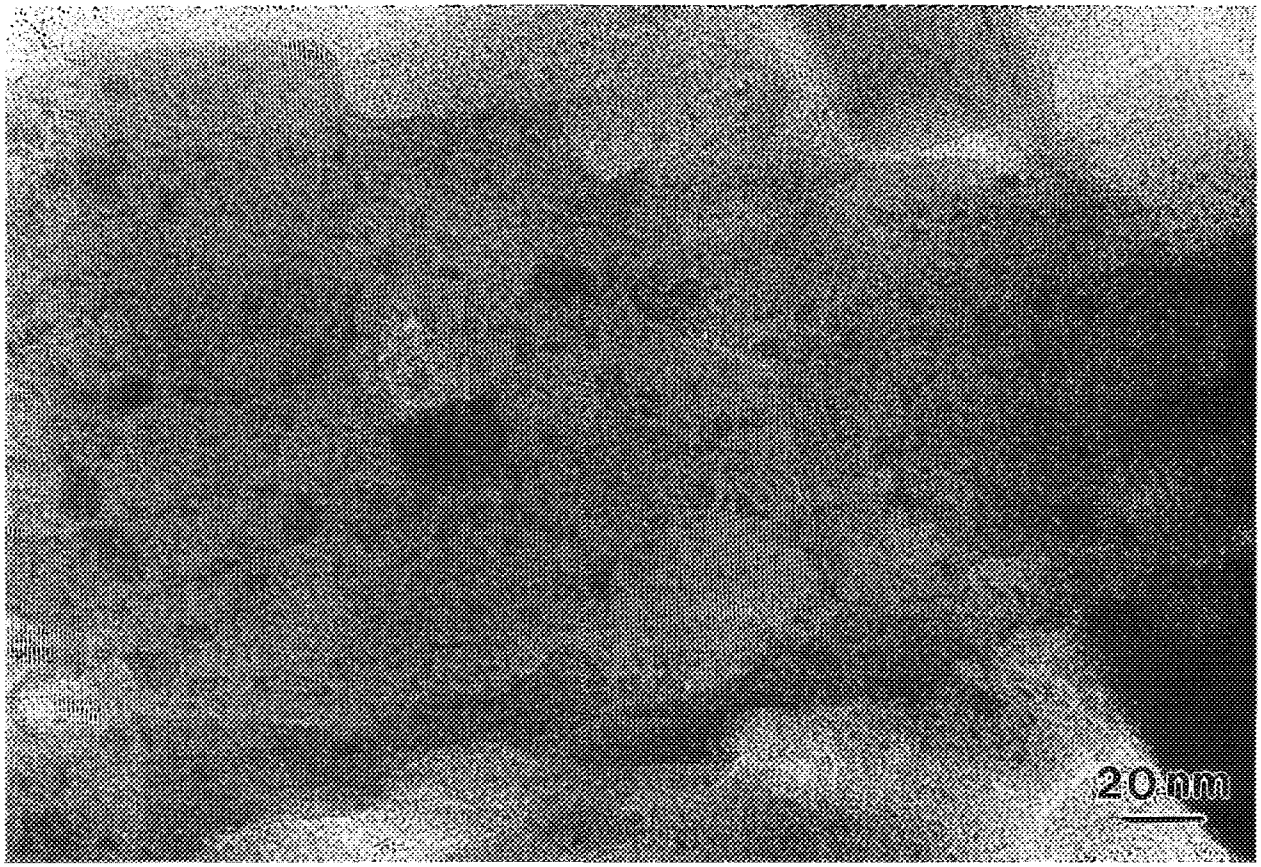

FIG. 7. High resolution electron micrographs showing lattice image of DBH molecular sieve with "darker" ferric molybdate regions.

analyses indicated that Fe and No are finely dispersed throughout the DBH. In addition, Fe and Mo are always associated with each other. In the calcined CVD Fe/Mo DBH in Fig. 5b, very small dark particles are apparent at lower magnifications, which have compositions similar to either $Fe_2(MoO_4)_3$ or $FeMoO_4$, as identified by EDXS analyses.

High-resolution electron micrographs (HREM) (Figs. 6a and 6b) of the fresh CVD Fe/Mo DBH clearly show that most Fe/Mo-rich domains (with a darker contrast) have a rod-like shape with diameters ranging from 1 to 10 nm. More significantly, these rod-like Fe/Mo-rich domains tend to be oriented along the two micropore channel systems as defined by the DBH framework. Figure 7 is the HREM micrograph of an area from the calcined CVD Fe/Mo DBH counterpart, which shows that the previous rod-like particles have rearranged into nearly spherical Fe/Mo rich particles. These particles are dispersed in the DBH with sizes ranging from 2 to 40 nm. Occasionally, larger Fe/Mo particles (greater than 50 nm in size) are observed, which are located exterior to the DBH particle. One such particle is shown on the right side of Fig. 5 (complete particle not shown). As indicated before, the Fe/Mo-rich particles are either $Fe_2(MoO_4)_3$ or $FeMoO_4$. The HREM observation provides clear insight into the pathway for the deposition of Fe and Mo during CVD, that is, via the two primary micropore channel system. This pathway of Fe/Mo deposition has a predominant effect in confining the Fe/Mo into the DBH in the final catalyst. Although the shape and size of the $Fe_2(MoO_4)_3$/$FeMoO_4$ particles have changed due to significant Fe and Mo migrations, the majority of the particles are dispersed within the DBH molecular sieve.

The processes of CVD deposition and calcination appear to introduce minor and localized destructions of the DBH crystalline structure, as shown in Figs. 6 and 7. However, the density of such localized defect regions is so small that macroscopically speaking, both fresh and calcined molecular sieves have nearly perfect crystalline structure. It is also interesting to note that the prolonged calcination process seems to have some healing effect on these localized defect regions, as suggested by the apparent overall lower density of defect regions in the calcined CVD Fe/Mo DBH.

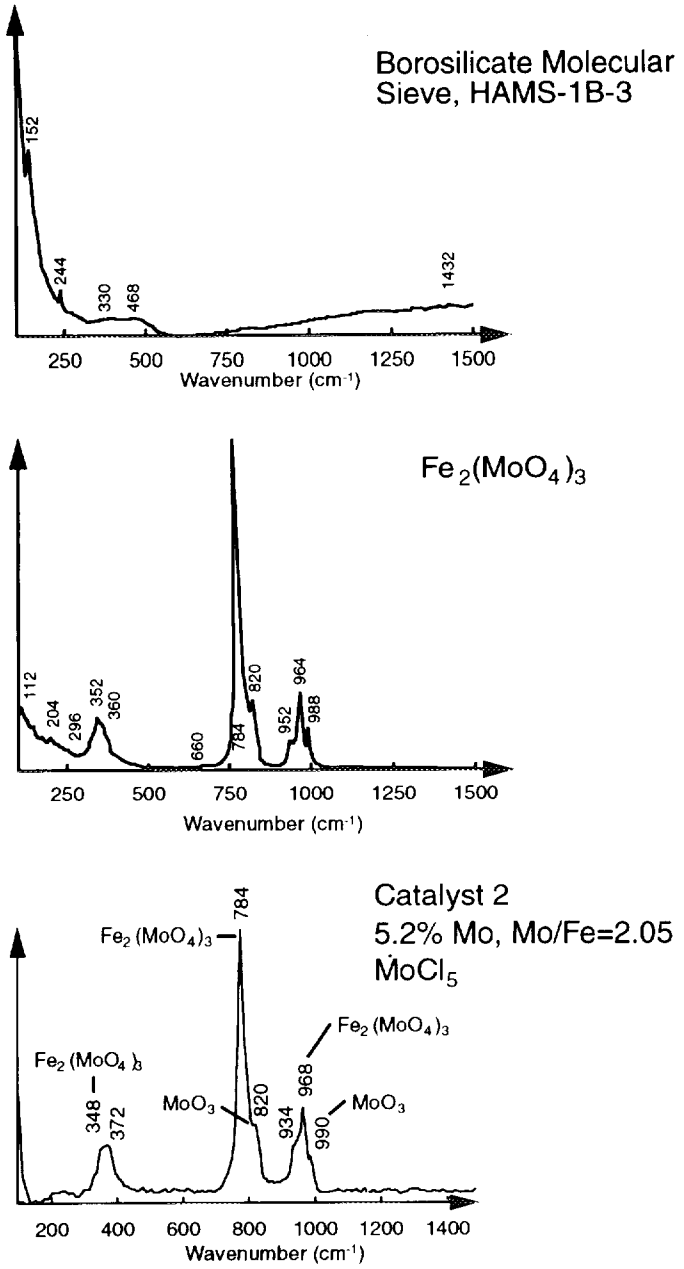

FIG. 8. Raman spectra of HAMS-1B-3, $Fe_2(MoO_4)_3$, and catalyst 2.

Raman Spectra Study

The Raman spectrum of the borosilicate molecular sieve, HAMS-1B-3, which contains 1900 ppm boron in the SiO_4 tetrahedral matrix, shows that only weak and broad features are detected in the region below 500 cm^{-1} as shown in Fig. 8. Meanwhile, the amorphous SiO_2 gives no Raman active bands. Since the catalyst components normally appear at 700–1000 cm^{-1}, Raman bands due to catalyst supports should not cause any spectral interference with the catalyst components.

Raman spectra of the catalyst 3 sample, the dried precursor to catalyst 4 (14 wt% Mo, Mo/Fe = 3.3), and the calcined final catalyst 4 (7 wt% Mo, Mo/Fe = 1.8) are shown in Fig. 9. The major Mo species detected are ferric molybdate at 964, 936, and 784 cm^{-1}, and MoO_3 at 992, 816, 664 cm^{-1} for catalyst 4. For its precursor, surface molybdate species, monomer $[MoO_4]^{2-}$ and polymeric molybdate, were also identified at 846 and 952 cm^{-1}, respectively. It is apparent that all of the surface molybdate species and part of MoO_3 were sublimated out of the system during the prolonged calcination at 650°C.

Catalyst 5, CVD Fe/Mo/ZSM-5, containing 5.3 wt% Mo, 2.21 wt% Fe, and Mo/Fe = 1.4 was further impregnated with ammonium paramolybdate to obtain catalyst 6. The resulting catalyst, catalyst 6, contains 8.9 wt% Mo, 2.47 wt% Fe, and Mo/Fe = 2.0. Raman spectra of catalysts 5 and 6 are shown in Fig. 10. In both samples, three principal species are detected, namely, $Fe_2(MoO_4)_3$ at 786 and 970 cm^{-1}, MoO_3 at 820 and 996 cm^{-1}, and α-Fe_2O_3 at 1324 cm^{-1}. The catalyst 6 sample shows a much-diminished α-Fe_2O_3 band and a much greater amount of MoO_3 relative to $Fe_2(MoO_4)_3$ than the original sample. It is likely that some portion of ammonium molybdate reacts with the ferric oxide to form $Fe_2(MoO_4)_3$, while the re-

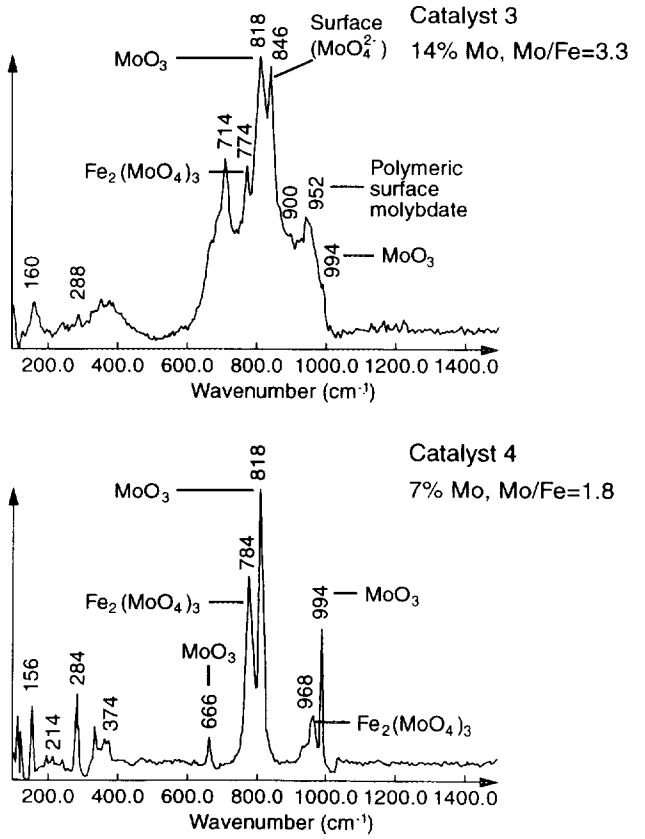

FIG. 9. Raman spectra of catalyst 4, CVD Fe/Mo/DBH, and catalyst 3 a precursor to catalyst 4.

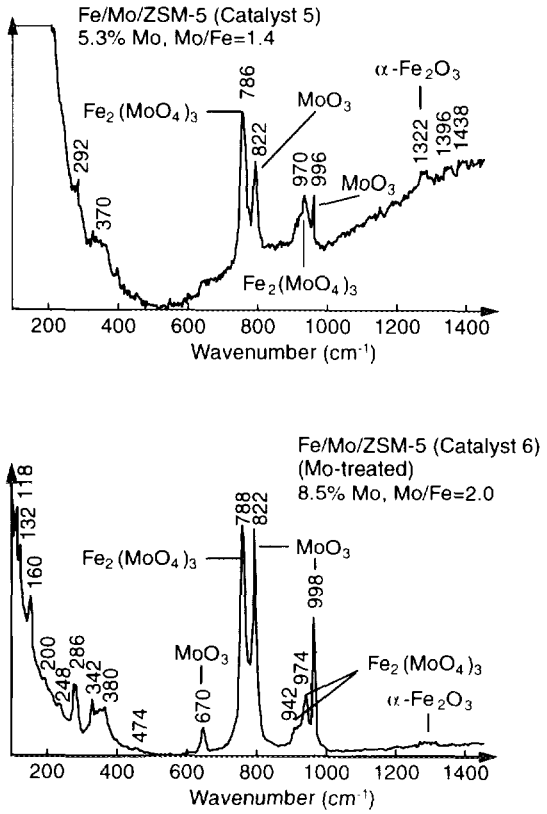

FIG. 10. Raman spectra of catalysts 5 and 6, CVD Fe/Mo/ZSM-5.

maining portion is retained on the ZSM-5 surface leading to formation of MoO_3 after calcination. Although the α-Fe_2O_3 phase was virtually gone in the treated sample, disproportionation of *p*-xylene to toluene and pseudocumene accompanied extensive burning with a limited amount of aldehyde formation.

XANES Study

The results of the electron yield core level spectroscopy of the dosed ferric molybdate are summarized in this section. The results of the CVD-prepared deboronated molecular sieve had a poorer signal to noise ratio reflected the same trends as those found in the pure ferric molybdate material. The carbon 1*s* spectrum of the CO_2 dosed ferric molybdate at 330°C is shown in Fig. 11 as a normalized (norm.) total electron yield after the background carbon signal is subtracted. The presence of carbon is ubiquitous throughout the optics of the 6*m* toroidal grating monochromator (TGM) so that the subtraction of the background carbon absorption is important. These data are compared to a spectrum of condensed (cond.) multilayer benzene at 125 K on gold. Comparison of the C 1*s* absorption data with published data for condensed CO_2 indicates a close correspondence (9, 10). The difference absorption data indicate for saturation CO_2 coverage the presence of CO_2 at reaction temperatures of 330°C.

The total electron yield data at the Mo $3d_{5/2,3/2}$ region are shown in Fig. 12. No noticeable differences are observed between the fresh ferric molybdate and after the 2.5-kL CO_2 dose at either 0 or 330°C. At the dosing temperature (−125°C) the total yield is suppressed and a poorer signal-to-noise ratio is observed. The total electron yield absorption data of the Fe $2p_{3/2},1/2$ are shown in Fig. 13. The observed spin–orbit splitting of 13.5 eV is consistent with a Fe^{3+} ion. The changes in the distribution of states before and after CO_2 dosing persist to reaction temperature (330°C). A plausible explanation of the observed redistribution of states could stem from the convolution of $2p_{3/2,1/2}$ with 3*d* unoccupied orbitals. The decrease in transition strength for the $2p \rightarrow 3d$ excitation might reflect a charge transfer interaction with the CO_2 which would reduce the number of unoccupied *d*-states.

A molecular model of the ferric molybdate indicates tetrahedral coordination of the Mo^{4+} ions and octahedral coordination of the Fe^{3+} ions. The CO_2 appears to preferentially interact with the 3*d* states of the Fe^{3+} ion and persists to reaction temperature (330°C) indicating a strong chemisorption state. A local cluster of ferric molybdate is represented in Fig. 14 about two octahedral Fe^{3+} sites surrounded in the second shell by the tetrahedrally coordinated Mo sites. The oxygen anions are deleted for clarity. The *p*-xylene molecular model is shown to scale. The size correspondence of the methyl-to-methyl group

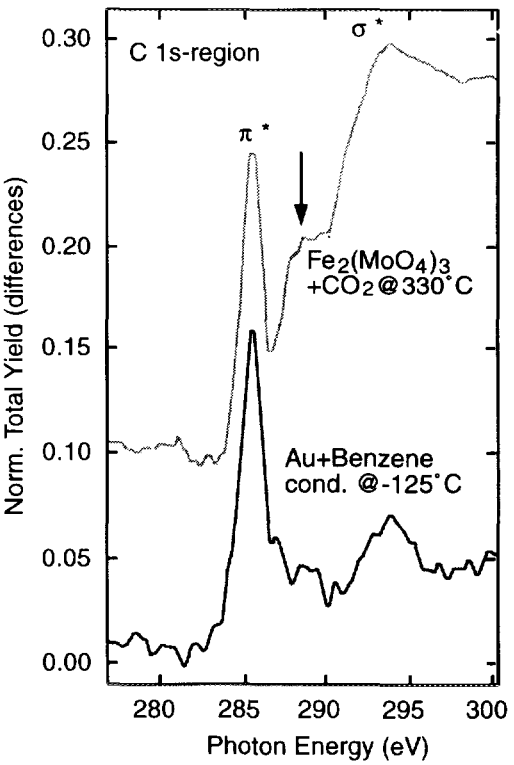

FIG. 11. C_{1S} X-ray absorption near edge spectroscopy, (XANES) taken at Synchrotron Radiation Center showing presence of CO_2 at 330°C after dosing at liquid nitrogen temperature.

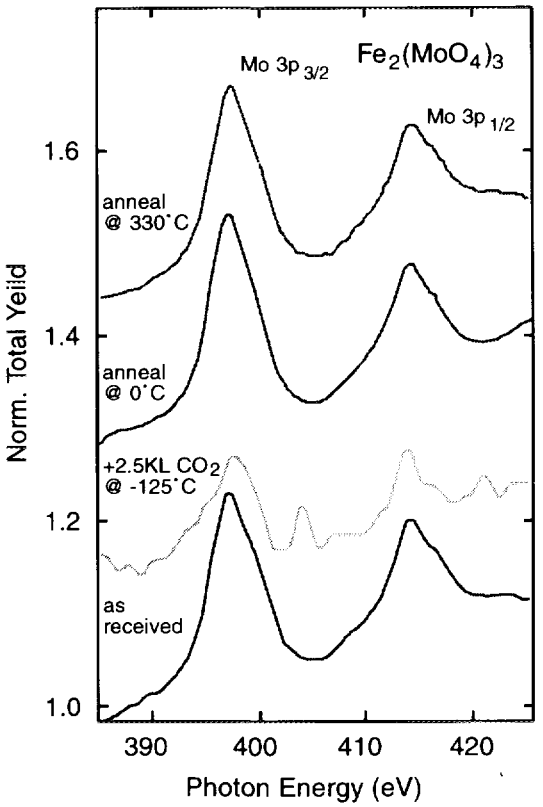

FIG. 12. $Mo^{+6}3p_{3/2,1/2}$ XANES showing minimal effect of CO_2 on $Mo^{+6}4d^*$ orbitals.

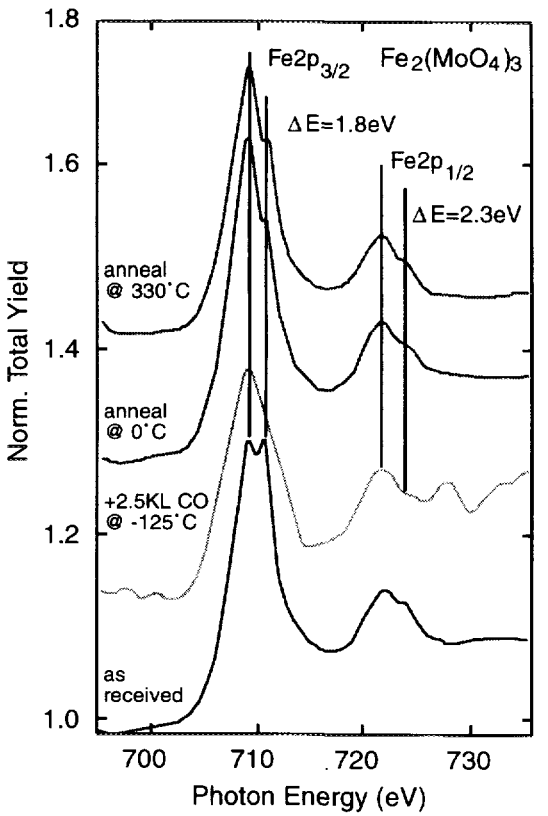

FIG. 13. $Fe^{+3}2p_{3/2,1/2}$ XANES indicating major effects of CO_2 on Fe^{+3} $3d^*$ orbitals.

of the *p*-xylene with the Mo–Mo distances and Fe–Fe distance supports the observation of two-site oxidation catalysis.

CONCLUSIONS

The Fe/Mo/DBH catalyst exhibited a stable *p*-selective oxidation activity to form terephthaldehyde with a high selectivity by the gas phase O_2 oxidation of *p*-xylene under mild reaction conditions. The catalyst also catalyzes other reactions, such as oxydehydrogenation, hydroxylation of benzene to phenol, and CO_2 activation. Two phases, $Fe_2(MoO_4)_3$ and MoO_3, were identified by Raman spectroscopy.

Combined techniques of analytical electron microscopy (AEM), high-resolution electron microscopy (HREM), Raman spectroscopy, X-ray powder diffraction, X-ray photoelectron spectroscopy, and *in situ* total electron yield near edge spectroscopy (XANES) were employed to characterize the catalyst. HREM studies revealed that during the CVD process Fe and Mo are deposited into the DBH molecular sieve via two micropore channel systems as defined by the DBH framework, resulting in a uniform dispersion of very small particles of either $Fe_2(MoO_4)_3$ or $FeMoO_4$. In the final catalyst, the majority of the $Fe_2(MoO_4)_3/FeMoO_4$ particles are confined on the DBH molecular sieve crystallites as a separate phase anchored on the DBH framework. X-ray diffraction techniques were used to study the starting composition mate-

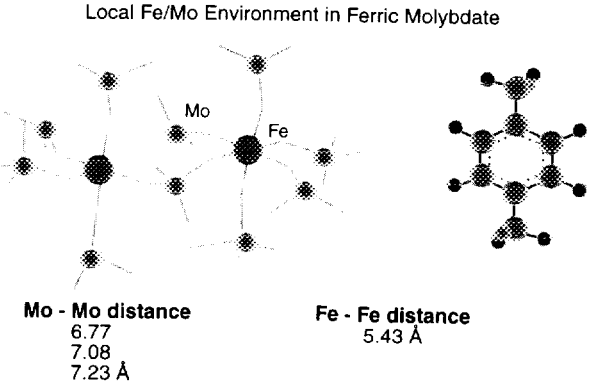

FIG. 14. Molecular model of ferric molybdate local cluster showing octahedrally coordinated Fe^{+3} and tetrahedrally coordinated Mo^{+6} ions. The superposition of *p*-Xylene indicates close size coorespondence of Mo–Mo-paired sites and size of *p*-Xylene molecule.

rial (before CVD on HAMS-1B) in the temperature range $20 < T < 450$°C. The starting material contains both ferric molybdate, $Fe_2(MoO_3)_4$, and molybdenum trioxide phases. The high-temperature experiments show the presence of a phase transition in the ferric molybdate phase. The transition has an onset at $T \approx 250$°C and is not complete even at 450°C. The enhancement of activity with the presence of CO_2 in the gas phase was addressed by *in situ* synchrotron radiation studies. *In situ* low-temperature CO_2 dosing XANES experiments provided evidence for a strongly chemisorbed CO_2 species on Fe/Mo/DBH at reaction temperature.

ACKNOWLEDGMENTS

We thank Brad Huggins for assistance in obtaining the EDXS data. The Raman spectroscopy studies were performed by J. Shyu. We also acknowledge S. Short for the X-ray diffraction data, and we thank Thanh Nguyen and Walter Nyderek for the X-ray photoelectron spectroscopy data.

REFERENCES

1. Pajda, E., *Chemik* (Gliwice) **23**(8), 291 (1970).
2. Yoo, J. S., Donohue, J. A., Kleefisch, M. S., Lin, P. S., and Elfline, S. D., *Appl. Catal. A: General* **105,** 83 (1993).
3. Yoo, J. S., Lin, P. S., and Elfline, S. D., Appl. Catal. A: General, **106,** 259 (1993).
4. Yoo, J. S., Donohue, J. A., and Kleefisch, M. S., *Appl. Catal. A* **110,** 75 (1994).
5. Yoo, J. S., *et al.*, to be published.
6. Yoo, J. S., Donohue, J. A., and Choi-Feng, C., submitted for publication.
7. Massarotti, V., Flor, G., and Marini, A., *J. Appl.* **14,** 64 (1981).
8. Plyasova, L., *J. Struct. Chem.* (USSR) **17,** 647 (1976).
9. Bader, M., Hillert, B., Puschmann, A., Hasse, J., and Bradshaw, A. M., *Europhys. Lett.* **5,** 443 (1980).
10. Illing, G., Heskett, D., Plummer, E. W., Frund, H.-J., Somers, J., Lindner, Th., Bradshaw, A. M., Starke, U., Heinz, K., De Andres, P. L., Saldin, D., and Pendry, J. B., *Surf. Sci.* **206,** 1 (1988).